Gharamti, I. E.; Dempsey, J. P.; Polojärvi, A.; Tuhkuri, J.

Fracture of warm S2 columnar freshwater ice

Published in:
Acta Materialia

DOI:
10.1016/j.actamat.2020.10.031

Published: 01/01/2021

Document Version
Publisher's PDF, also known as Version of record

Acta Materialia 202 (2021) 22–34

Contents lists available at ScienceDirect

Acta Materialia

journal homepage: www.elsevier.com/locate/actamat

Fracture of warm S2 columnar freshwater ice: size and rate effects

I.E. Gharamti[a,*], J.P. Dempsey[b], A. Polojärvi[a], J. Tuhkuri[a]

[a] Department of Mechanical Engineering, Aalto University, Espoo 00076, Finland
[b] Department of Civil and Environmental Engineering, Clarkson University, Potsdam, NY 13699, USA

ARTICLE INFO

Article history:
Received 23 June 2020
Revised 14 October 2020
Accepted 16 October 2020
Available online 20 October 2020

Keywords:
Freshwater S2 ice
fracture
size effect
rate effect
viscoelasticity

ABSTRACT

Large scale laboratory experiments on size and rate effects on the fracture of warm columnar freshwater ice have been conducted with floating edge-cracked rectangular plates loaded at the crack mouth. The largest test plate size had dimensions of 19.5m x 36m. The overall crack-parallel dimension covered a size range of 1 : 39, possibly the largest for ice tested under laboratory conditions. The loading rates applied led to test durations from fewer than 2 seconds to more than 1000 seconds, leading to an elastic response at the highest rates to a viscoelastic response at the lower rates. Methods for both the linear elastic fracture mechanics (LEFM) and a non-linear viscoelastic fictitious crack model (VFCM) were derived to analyze the data and calculate values for the apparent fracture toughness, crack opening displacement, stress-separation curve, fracture energy, and size of the process zone near a crack tip. Issues of notch sensitivity and minimum size requirements for polycrystalline homogeneity were addressed. Both size and rate effects were observed, as well as how these two factors are interrelated in the fracture of columnar freshwater ice. There was a size effect at low rates but no size effect at high rates. There was a rate effect for the larger test sizes but a weaker or no rate effect for the smallest test size.

1. Introduction

The importance of ice mechanics and arctic marine technology is increasing due to climate change. Warming of the Arctic has led, and will lead, to changes in the ice conditions: in the future we will have less ice than today and the ice will be thinner, warmer, weaker, and more fragmented. These changes will have major impact on the Arctic environment and to the marine operations in the area. As an example, as the ice loads on ships and marine structures result from the failure process of ice, the design and safe operations require understanding of fracture processes of different ice features in the changing conditions. As a further example, modelling the fragmentation of the arctic sea ice requires that the crack propagation be modelled.

The fracture behaviour of ice is affected by a number of factors including grain size and type, loading rate, temperature, polycrystallinity, loading direction, and test plate size. By conducting large-scale in-situ fracture experiments with sea ice, Dempsey et al. [1,2] eventually questioned the applicability of a one parameter fracture mechanics for sea ice, ultimately favoring a viscoelastic fictitious crack model. These, and other, observations led to the suggestion that the fracture of small and large ice specimen may not be similar, and that the applicability of LEFM to even freshwater ice may be limited. At the core of this discussion is the requirement of LEFM that the material behaviour is linearly elastic except in a small area near a crack tip [2,3]. Qualitatively, it can be argued that these conditions prevail when the the loading rate is high and the specimen is large. Quantitatively, we know little as to what is a high rate, how large is a large specimen, and how these two questions are affected by temperature, size and type of the ice (granular or columnar), and other parameters.

A fundamental concern in this study was that a one parameter fracture mechanics might prove not useful for warm S2 columnar freshwater ice [2]. While the viscoelastic fictitious crack model had proved useful for first-year sea ice [2], it is unknown if it can model the fracture of S2 columnar freshwater ice. At the outset, the requisite test size for polycrystalline homogeneity for large grained columnar freshwater ice is also unknown. Polycrystalline homogeneity requires that the crack length and the uncracked ligament are significantly larger than the grain size, and the specimen contains sufficient number of grains to be regarded as homogeneous [3–5]. As discussed by Dempsey et al [6], polycrystallinity is an issue with large grained ice. In order to address these questions

* Corresponding author.
E-mail addresses: iman.elgharamti@aalto.fi (I.E. Gharamti), jdempsey@clarkson.edu (J.P. Dempsey), arttu.polojarvi@aalto.fi (A. Polojärvi), jukka.tuhkuri@aalto.fi (J. Tuhkuri).

https://doi.org/10.1016/j.actamat.2020.10.031

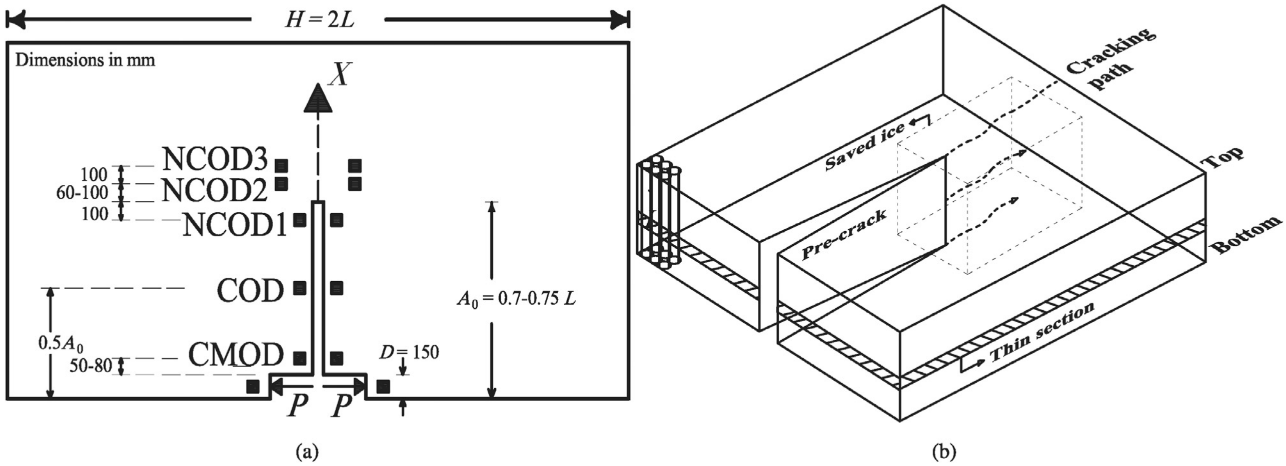

Fig. 1. (a) The edge cracked rectangular plate of width H, length L, and crack length A_0 used in the experiments. (b) The crack orientation and direction of crack propagation; also the columnar grains are shown. The dotted rectangular box represents the ice cut for storage and analysis.

and study the size and rate effects on the fracture of S2 columnar freshwater ice, in-situ edge-cracked rectangular plates of floating ice have been split (Fig. 1), with the crack parallel dimension ranging from 0.5 m to 19.5 m (representing a size range of 1:39). While field work with ice provides results from a natural material in the real environment, laboratory studies allow a control of test parameters not possible in the field. The ice thickness ranged between 35 cm and 41 cm. The experiments were conducted at the Aalto Ice Tank and all the specimens were from a single large ice sheet to ensure the same grain size and structure for all the tests. The Aalto Ice Tank is the largest square basin available for use. This size range of 1 : 39 may be the largest achieved for ice under laboratory conditions. During the experiments the ambient temperature in the laboratory was kept at -2 C in order to study fracture of warm ice, but also to avoid a temperature gradient in the ice. Except specimen size, loading rate, and the gradually increasing thickness, all ice and test parameters were constant. The experiments were analysed by using two approaches: a one-parameter linear elastic fracture mechanics approach and a multi-parameter non-linear viscoelastic approach.

Large scale in-situ fracture experiments studying size and rate effects with freshwater S2 ice have not been conducted before and the stress-separation curve for this type of ice has not yet been determined. The largest test sizes in the earlier studies have been of the size of the smallest test size used here and most of the earlier studies have tested crack parallel dimensions of tens of centimeters. The general focus of the previous work with freshwater ice has been to characterize the mode I fracture behavior in terms of fracture toughness using LEFM [7–24]. Dempsey has provided a summary of the experimental work on fracture of freshwater ice and suggested that many laboratory test sizes may have been too small in terms of the requirement of linear elastic fracture mechanics [3]. It is important to note that a scale effect may not occur unless the specimen sizes themselves are large enough [25].

The rest of the paper is structured as follows. In Section 2, descriptions of the ice growth, the experimental setup, and the ice properties are presented. In section 3, linear elastic fracture mechanics is applied as a one-parameter fracture mechanics approach to derive the expression of the apparent fracture toughness. Section 4 introduces a non-linear viscoelastic fictitious crack model and explains how it is used to analyze the experiments. The experimental and model results with the notch sensitivity and homogeneity analysis are presented in Section 5 and discussed in Section 6. Section 7 ends the paper with conclusions.

2. Experiments

2.1. Ice growth, thickness, and temperature

A sheet of freshwater S2 ice was grown in the Aalto Ice Tank, a 40 m x 40 m, 2.8 m deep water basin equipped with a cooling system. S2 ice is columnar polycrystalline ice with a random and horizontal c-axis orientation in most of its grains [26]. The growth process was initiated by lowering the air temperature in the ice tank to −14 C and bubbling air into the water to obtain a uniform water temperature. When a water temperature of 0.2 C was reached, the air bubbling system was shut off and after approximately 15 minutes a fine mist of water droplets, at around +2 C, was sprayed into the air above the basin. Once the droplets reached the water surface, they acted as nuclei for ice crystals to form.

After four weeks at −14 C, the initial seeded ice layer had developed into a sheet of bubble-free columnar S2 ice with a thickness of approximately 34 cm. For the experiments, the ambient temperature was raised to −2 C and maintained at that temperature. As the test program lasted about a month, the ice sheet grew from the 34 cm to 41 cm during the test program. The ice thickness at the crack tip was measured before each test and is reported in Table 1. After completing each experiment, a through-the-thickness block of ice was cut from both sides of the crack path as illustrated by the dotted rectangular box in Fig. 1b. These blocks extended from 5 cm behind up to 15 – 35 cm ahead of an initial crack tip and allowed the measurement of thickness profiles along the crack paths: the ice thickness varied only a few millimeters along each crack path. The ice blocks studied were clear and transparent, there were practically no air bubbles. The ice blocks were stored in triple plastic bags to prevent sublimation and placed in freezers operating at -20 C. Care was taken to mark the correct orientation of the blocks.

The vertical temperature profile of the ice sheet was measured daily, at different locations in the ice sheet. The ice temperature varied more or less linearly with depth but did not vary much during the test program. It is worth emphasizing that the tested ice temperature, −0.3 C at the top surface, is warm in comparison to the majority of laboratory tests performed to date.

2.2. Grain size and c-axis orientation

The microstructure of the ice was analysed by making and studying thin sections in a cold room. The conventional way of

Table 1
Specimen dimensions, measured data, and results computed using linear elastic fracture mechanics.

Test	L m	H m	A_0 m	h cm	E_{CMOD} GPa	E_{COD} GPa	$P_{\max}$ kN	t_f s	σ_n MPa	K_Q kPa$\sqrt{\mathrm{m}}$	$\dot{K}$ kPa$\sqrt{\mathrm{m}}\mathrm{s}^{-1}$	CMOD μm	$\dot{\mathrm{CMOD}}$ $\mu\mathrm{ms}^{-1}$	NCOD1 μm	$\dot{\mathrm{NCOD1}}$ $\mu\mathrm{ms}^{-1}$
RP1	0.5	1	0.35	35	6.9	-	1.7	54.9	0.486	126.2	2.298	33.1	0.602	5.2	0.094
RP2	0.5	1	0.35	35	6.9	-	2.3	51.9	0.657	168.6	3.247	43.3	0.834	7.5	0.145
RP3	0.5	1	0.35	37.1	6.4	-	1.6	1.9	0.431	108.4	57.058	29.1	15.321	7.8	4.128
RP4	0.5	1	0.35	37.6	7.0	-	1.9	20.8	0.505	129.2	6.223	37.6	1.811	3.2	0.154
RP5	0.5	1	0.35	40.2	7.3	-	2.1	571.7	0.522	132.2	0.231	36.1	0.063	3.4	0.006
RP6	0.5	1	0.35	41.1	5.6	-	2.4	811.4	0.584	145	0.179	59.5	0.073	10.4	0.013
RP7	3	6	2.1	34.5	6.0	6.2	4.6	86.9	0.259	159.4	1.834	236	2.716	47.2	0.543
RP8	3	6	2.1	34.5	6.6	-	3.0	2.7	0.169	106	39.259	157	58.148	22.9	8.482
RP9	3	6	2.1	34.5	6.1	6.2	5.2	148.0	0.293	180.6	1.221	266	1.798	42.8	0.289
RP10	3	6	2.1	34.5	6.7	6.7	4.8	222.2	0.271	166.8	0.751	215.6	0.970	34.6	0.156
RP11	3	6	2.1	36	7.4	7.7	4.2	15.3	0.227	139.4	9.091	174.4	11.374	25.2	1.644
RP12	3	6	2.1	37.2	5.7	5.9	6.8	701.8	0.355	221.3	0.315	370.5	0.528	68.5	0.098
RP13	3	6	2.1	37.6	4.7	4.8	5.7	1027.1	0.295	184.3	0.179	420.3	0.409	63.4	0.062
RP14	19.5	36	14.6	35	5.7	5.7	10	213.5	0.127	186.0	0.871	961.7	4.505	37.2	0.174

thinning ice with a microtome was replaced by a milling machine. The milling machine proved to be successful in producing a good quality surface finish, saving the long working hours with a microtome, and generating larger thin sections than with a microtome. In this method, ice sections were frozen on a plexiglass plate, instead of a glass plate. The plexiglass used has as good optical properties as glass, if not better, and is safer. The ice froze fast to the plexiglass and formed a strong bond. With the milling machine, the thickness of the ice sections was reduced to about 0.8 mm. The thin sections were then examined and photographed under cross-polarized light. Figs. 2a and 2c show horizontal and vertical sections, respectively, displaying the crystalline and columnar structure of the ice. The grain size was estimated by using the uniform-sphere-assumption method [27]. The grain size varied between 3 mm at the top and 10 mm at the bottom portion of the ice sheet. The mean grain diameter was 6.5 mm.

An examination of the c-axis orientation was carried out by analyzing hundreds of grains at different locations and depths along the ice sheet. The c-axis orientation plot from horizontal thin section (Fig. 2a) taken from the middle of the ice sheet is shown in Fig. 2b. The Schmidt net consists of 100 poles of the basal planes measured with a four-axis universal Rigsby stage. Refraction corrections [28] were applied for the universal stage measurements. In the type of axis projection plot used [29], a horizontal c-axis would be on the circumference and a vertical c-axis would be at the center. It can be seen that the c-axes of the columnar grains were randomly horizontal. The ice sheet had the same type of textural features throughout the depth and for the whole ice sheet: the ice was columnar S2 ice.

2.3. Specimen preparation and experimental procedure

An edge-cracked rectangular plate configuration with displacement controlled loading at the crack mouth was used (Fig. 1). Fourteen fracture tests were conducted with different loading rates and three test sizes: 19.5m x 36m, 3m x 6m, and 0.5m x 1m (Table 1).

The specimens were cut from the parent ice sheet with an electric chain saw. The kerfs around each plate were kept clear of ice by using shovels. Initial cracks with length A_0 were also cut with the electric chain saw giving a crack of width 8 mm. Directly before each test a sharp crack tip was produced using either a carpet knife with a blade width of 0.71 mm, or a hand saw with a blade width of 1.21 mm. The length of the sharpened crack was $\approx 0.7 - 0.75\ L$,where $L$is the crack-parallel side length. The final sharpening nucleated microcracks along the crack front, which effectively created a very sharp and more realistic crack tip. No significant blunting of the tip occurred during the test. The plane of the crack was perpendicular to the plane of the ice sheet; the crack front was vertical as shown in Fig. 1b. The parent ice sheet was kept intact, and each new test piece was cut from the parent ice sheet on an as needed basis.

A closed-loop servo-controlled hydraulic loading device was installed in a rectangular slot cut at the crack mouth to apply pressure on the crack faces (Fig. 1a). The tests were displacement controlled with the feedback signal measured along the loading device. The length of the contact between ice and the loading device ($D = 150$ mm) was the same for each test size and was chosen to keep the contact pressure below 0.5 MPa to avoid crushing of the crack faces. In other words, the length of contact of the loading device $D$was not scaled with test size.

Direct measurement of the crack opening displacements was carried out using inductive displacement transducers (LVDTs) positioned at six different locations (Fig. 1): at the centerline of the loading device (the control displacement), at the crack mouth (CMOD), at about half the length of the crack (COD), 10cm behind the initial sharpened crack tip (NCOD1), $6 - 10$ cm ahead of the tip (NCOD2), and 20 cm ahead of it (NCOD3). NCOD denotes near-crack-tip opening displacement. LVDTs with a measuring range of $0 - 2$ mm and a resolution of less than 3 μm were used. In addition, parallel LVDTs with a larger range were used as secondary sources of data and as backup. No major discrepancies between the primary, high resolution, transducers and the secondary transducers were observed. All the LVDTs were mounted on 14.5 mm diameter wooden sticks that were frozen into holes in the ice, on both sides of the crack. The positions of the LVDTs, including the elevation above the ice surface, were kept constant for all the tests. The data was sampled at 1000 Hz.

In all the tests, the cracks propagated more or less straight, approximately along the x-axis and through the gauges NCOD2 and NCOD3, as illustrated by the dotted crack path in Fig. 1b. The aspect ratio ($H/L = 2$) used in the tests apparently supports crack path stability.

2.4. Fractographic examinations

The ice samples cut from both sides of the crack path were used to study the crack propagation by making horizontal thin-sections as sketched in Fig. 1b. Some of the ice samples were cut immediately after an experiment, others were cut one or two days after an experiment. As a result, the crack healed in some samples, and in other samples, the right and left sides of the crack were unattached. It was easy to make thin sections with a healed crack. For unhealed cracks, the two halves of the specimen were matched, and the matched sections were analyzed. The thin sections covered almost the whole crack path and provided numerous grains to study if a crack propagated through a grain or along a

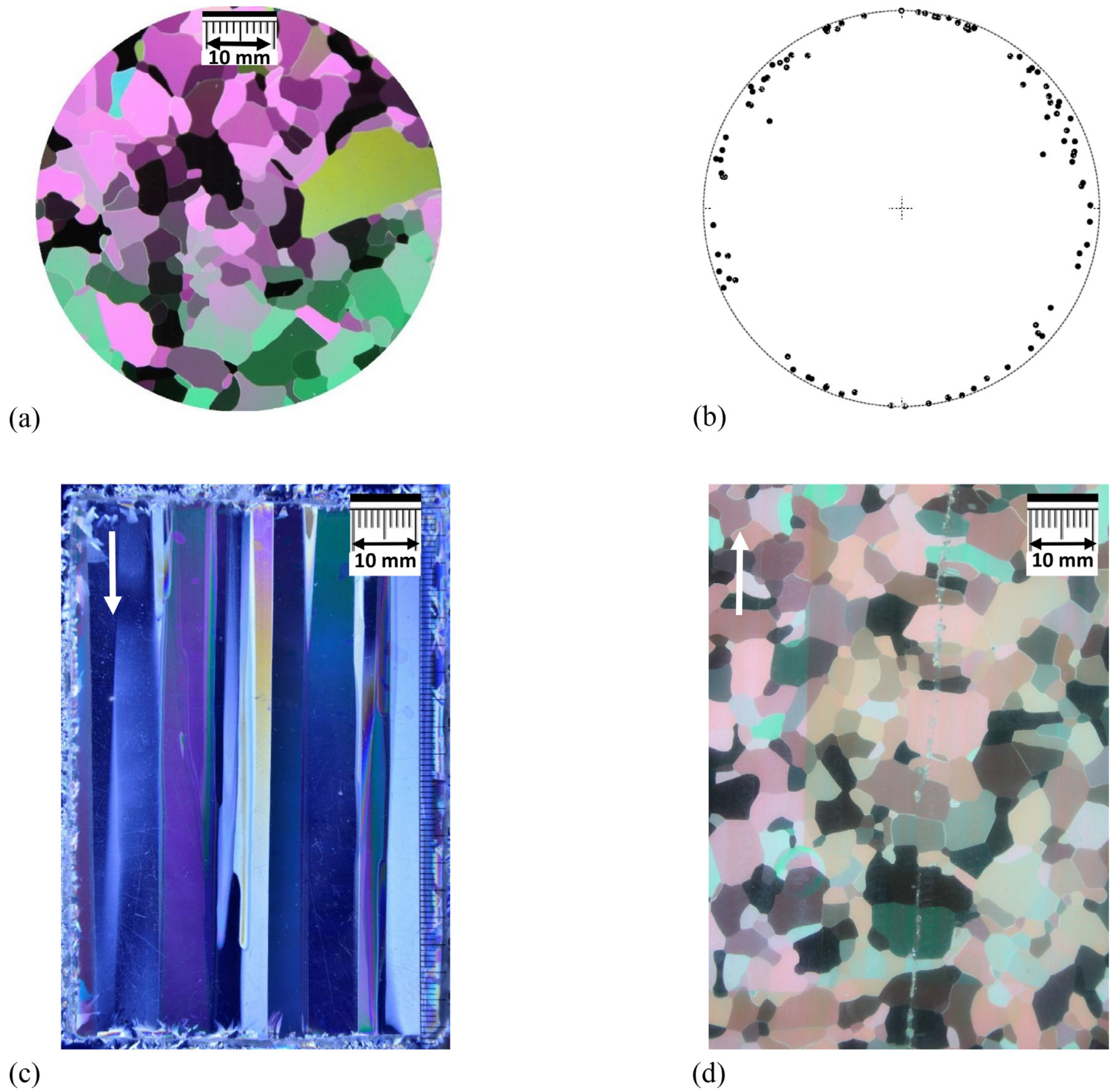

Fig. 2. (a) Horizontal thin section taken from the middle of the ice sheet and (b) its corresponding c-axis orientation Shmidt net. The plot consists of 100 poles of the basal planes measured by a four-axis universal Rigsby stage. (c) Vertical thin section showing columnar freshwater ice at the bottom of the ice sheet. The arrow indicates the growth direction. (d) Horizontal thin section showing a crack path and taken from a depth of 24 cm from the top of the ice sheet. The arrow indicates the direction of crack propagation. Vertical and horizontal thin sections were photographed between crossed polaroids.

grain boundary. It is obvious from Fig. 2d that transgranular fracture was dominant: the cracks propagated through the grain for almost all the grains.

3. Linear elastic fracture mechanics model

Expressions for stress intensity factor and crack opening displacement for the edge loaded, edge cracked rectangular plate used in the present experiments (Fig. 1a) are derived by following the weight function approach in [30]. The crack face pressure P/Dh is applied between $0 < X \leq D$, where P is the applied force by the loading device, D the length of contact between ice and the loading device, h the ice thickness, and X the position along the crack.

If the critical stress intensity factor (the fracture toughness) is test size independent and test geometry independent, it can be denoted by K_{Ic}. Because of the lack of standards for determining the proper specimen size, loading rate, etc. for the fracture toughness testing of ice, Dempsey [3] suggested the notation of apparent fracture toughness K_Q instead of K_{Ic}. Then $K(A_0) = K_Q$ when $P = P_{\max}$, where A_0 is the crack length. Eq. (1) in [30] leads to

$$K_Q = \frac{P_{\max}}{dh\sqrt{L}} \sqrt{\frac{2a_0}{\pi}}\, Z_1(d, a_0) \tag{1}$$

where L is the crack-parallel side length of the rectangular plate (Fig. 1a), $d = D/L$, $a_0 = A_0/L$, and $Z_1(d, a_0)$ is given by Eq. (A4) in Appendix A. For $d < x < a_0$ with $x = X/L$, the expression for the crack opening displacement (COD) follows from Eq. (1) in [30] as

$$E\,\delta = \frac{2P}{\pi\, dh} \left\{ \int_x^{a_0} Z_1(d, \eta) Z_2(x, \eta) d\eta \right\} \tag{2}$$

$Z_2(x, \eta)$ is defined by Eq. (A5) in Appendix A.

4. Viscoelastic fictitious crack model

Linear elastic fracture mechanics is limited to situations where material behavior is linearly elastic and where any process zone at the crack tip is small compared to other dimensions of the specimen. A popular model that addresses nonlinear fracture behavior

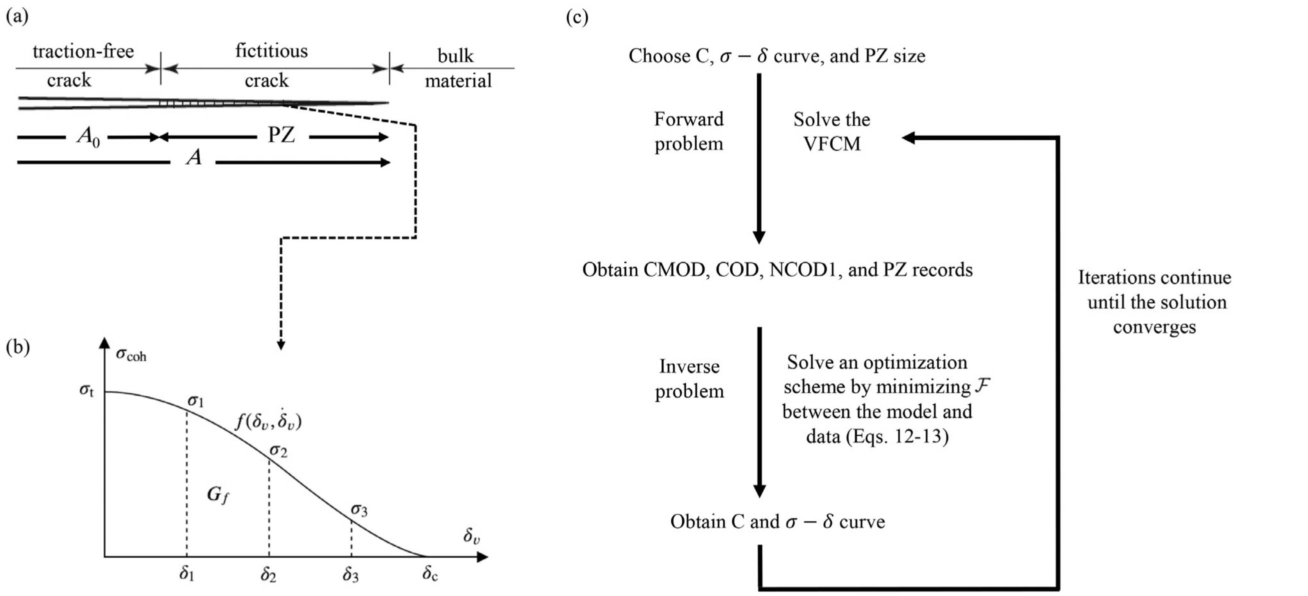

Fig. 3. (a) Illustration of the fictitious crack model. (b) Stress-separation curve describing the behavior in the PZ and showing the control points (see Eq. 4) used in the optimization procedure. (c) A flowchart illustrating the forward and inverse problems used for matching the experimental and model results.

and large process zones is the cohesive zone model or the fictitious crack model (FCM) [31]. The FCM has proved successful in modeling the fracture behavior of several quasi-brittle materials. The key idea of the FCM is the concentration of all nonlinear fracture mechanisms into a localized process zone, located on the crack line, as shown in Fig. 3a, where the length of a traction free crack is denoted as A_0 and the total length of a crack – including the process zone – as A,giving a length of the process zone as PZ = $A - A_0$. The crack-opening displacement at $X = A_0$ is denoted as δ_0. The behavior inside the process zone is described by a constitutive relation, known as the stress-separation law ($\sigma - \delta$ law), which relates the softening stresses to the crack-opening displacements, as shown in Fig. 3b. The response outside the process zone is governed by an applicable constitutive relation of the bulk material. In the present work, the viscoelastic fictitious crack model (VFCM) formulated by Mulmule and Dempsey [32] is adopted to model the response of the freshwater fracture tests conducted. The VFCM couples the FCM with the assumption that the behavior of the bulk material is linearly viscoelastic. However, for the freshwater ice fracture experiments conducted, neither the stress-separation law nor the viscoelastic material parameters are known before the experiments, but need to be back-calculated by requiring that the results from the experiments and from the modeling match.

The main elements that characterize the cohesive model are shown in Figs. 3a and 3b: the length of the process zone (PZ), the maximum cohesive stress ($\sigma_{\rm coh}$) that the material in the process zone can transfer and which initiates the growth of the process zone (tensile strength, σ_t), the critical displacement beyond which the material is fully separated and can transfer no more stresses (δ_c), the shape of the $\sigma - \delta$ curve, and the fracture energy represented by the area under the $\sigma - \delta$ curve. Fig. 3b represents a $\sigma - \delta$curve obtained under conditions in which a fully-developed-process-zone (FDPZ) has formed. The full fracture energy (G_f) is consumed. A FDPZ is achieved when two conditions are satisfied at $X = A_0$: $\sigma_{\rm coh} = \sigma_t$ and $\delta_0 = \delta_c$. Based on the testing conditions (load control versus displacement control, ice temperature, operating deformation mechanisms, etc.), either a full or a portion of the $\sigma - \delta$ curve / fracture energy can be obtained. Different approaches have been proposed to quantify the softening law. A pure experimental method would involve stable tensile tests to determine the parameters of the $\sigma - \delta$ curve. However, this approach has proven difficult and few reliable results have been obtained [33]. Instead, indirect methods, typically through a combined experimental-numerical procedure, have been employed both in concrete and ice research and proved promising [32,33]. These techniques apply inverse analysis in an iterative procedure to obtain the softening curve of the FCM. An iterative approach is also used here and the method is outlined below.

In this study, the creep compliance $J = 1/E + Ct^{1/2}$ is used to characterize the viscoelastic behavior of the bulk material, where E is the short-time elastic modulus measured at the crack mouth, C is the creep compliance constant, and t is the time. The form chosen for J is based on laboratory-scale experiments [34,35] conducted on saline ice at -10 C under a low compressive stress (0.5 MPa). Here, E is obtained from the initial linear portion of the load - crack mouth opening displacement plot and C through the iterative procedure described below.

According to the spirit of the FCM, the growth of the process zone is governed by the interaction of an externally applied load and the cohesive stress such that the resultant stress intensity factor vanishes at the fictitious crack tip.

The relation between the cohesive stress, the viscoelastic crack opening displacement, and the rate of the crack opening displacement is given by the stress-separation curve, shown in Fig. 3b, as follows,

$$\sigma_{\rm coh}(\delta_v, \dot{\delta}_v) = \begin{cases} f(\delta_v, \dot{\delta}_v) & 0 \le \delta_v < \delta_c \\ 0 & \delta_v \ge \delta_c \end{cases} \tag{3}$$

where δ_c and $\dot{\delta}_v$ represent the critical crack opening displacement and the rate of crack opening, respectively. Details of the VFCM equations outlined above are explained in [32].

To complete the viscoelastic fictitious crack model for freshwater ice, an iterative procedure was implemented. The availability of the load history and the displacement histories at different positions along the crack allows to carry an inverse analysis and to back-calculate the stress-separation ($\sigma - \delta$) law, the value of the creep compliance constant (C), and the length of the process zone (PZ) (Figs. 3a and 3b). At each iteration, two problems are solved, forward and inverse. In the forward problem, values for

$\sigma-\delta$curve, C, and PZ are initially assumed – and later obtained though optimization – and the viscoelastic fictitious crack model is solved to obtain the crack opening profile and the length of the process zone. The measured load - time record is applied in discretized steps into the model. This provides displacement results at different positions along the crack, including the process zone, through an experiment. The length of the process zone is obtained from the requirement that the stress intensity factor is zero at the fictitious crack tip. In the inverse problem, the crack opening profile is assumed to be known, and an optimization scheme using the Nelder-Mead (N-M) algorithm [36] is used to obtain the constitutive parameters (C and the $\sigma-\delta$ law) by minimizing the difference between the numerical data and the experimental data. Once the $\sigma-\delta$ law and C are solved, they are used as input in the forward problem and the iteration continues until the best attainable agreement is obtained. A flowchart illustrating the implemented procedure is shown in Fig. 3c.

In the optimization scheme, five control pairs, shown in Fig. 3b, are used to define the $\sigma-\delta$ curve:

$$\begin{Bmatrix} \delta = 0, & \delta_1, & \delta_2, & \delta_3, & \delta_c \\ \sigma = \sigma_t, & \sigma_1, & \sigma_2, & \sigma_3, & 0 \end{Bmatrix} \tag{4}$$

in which δ_1,δ_2, and δ_3 are assumed such that $\delta_1 < \delta_2 < \delta_3 < \delta_c$, and the N-M scheme optimizes the control points, δ_c,σ_t,σ_1,σ_2, and σ_3. The $\sigma-\delta$law was back-calculated without any assumption about its shape. The optimization scheme minimizes an objective function $\mathcal{F}$ given by the norm of a residual

$$\mathcal{F} = \underset{\delta_c,\sigma_t,\dots}{\arg\min} \sum_{i=1}^{N=45} \left\| M_i(\delta_c, \sigma_t, \sigma_1, \sigma_2, \sigma_3, C) - D_i \right\|_2 \tag{5}$$

where $M_i$and D_i refer to the displacement values given by the model and obtained by using the experimental data, respectively. $\|.\|_2$ is the Euclidean norm of a vector. The displacement values that are matched total to 45: CMOD, COD, and NCOD1 (Fig. 1a) at 15 time instances during the loading. As no LVDT was placed at the initially sharpened crack tip, it was decided to match the displacement values given by NCOD1.

In the current problem, the objective function $\mathcal{F}$ is numerical, and accordingly, no closed form solution for the gradient of the objective function is available. Derivative-based optimization methods such as Newton solvers cannot be used. This is the main motive behind the selection of the Nelder-Mead (N-M) method, which is a derivative-free optimization method [36].

The optimization problem has constraints: the cohesive stresses are tensile and have a softening behavior (Fig. 3b). Besides, upper and lower bounds were provided for the arguments. The bounds for the cohesive stresses were based on the tensile strength of columnar freshwater S2 ice [37–39], for the critical crack opening displacement on the measured displacements at NCOD1 and NCOD2 in each experiment, and for the creep compliance constant on sea ice fracture studies [2].

5. Results

5.1. Linear elastic fracture mechanics analysis

Table 1 gives the dimensions of the ice samples together with the measured and computed results. The apparent fracture toughness (K_Q) was computed from the failure load and dimensions by using Eq. (1). The loading rate ($\dot{K}$) was computed by dividing K_Q by the time to failure (t_f). The time to failure varied from about 2 seconds to about 1000 seconds giving a loading rate range of $0.18 \cdots 57$ kPa$\sqrt{\text{m}}\,\text{s}^{-1}$. The elastic moduli ($E_{CMOD}$) and ($E_{COD}$) were computed by Eq. (2) from the initial linear portion of the load - CMOD displacement records and load - COD displacement records, respectively. Some of the E_{COD} values are missing, caused by the fact that the initial portion of the associated load-COD curve was very noisy. No significant difference in the moduli was found. Displacements at the crack mouth and near the crack tip at the crack growth initiation, CMOD and NCOD1 respectively, were measured at locations shown in Fig. 1a. $\dot{\text{CMOD}}$ and $\dot{\text{NCOD1}}$ indicate the displacement rates and were obtained by dividing CMOD and NCOD1 by the time to failure. Attempts were made to measure displacements ahead of the crack also (Fig. 1a), but those displacements were very small and the measurements failed especially for small specimens and fast tests and are not analysed here.

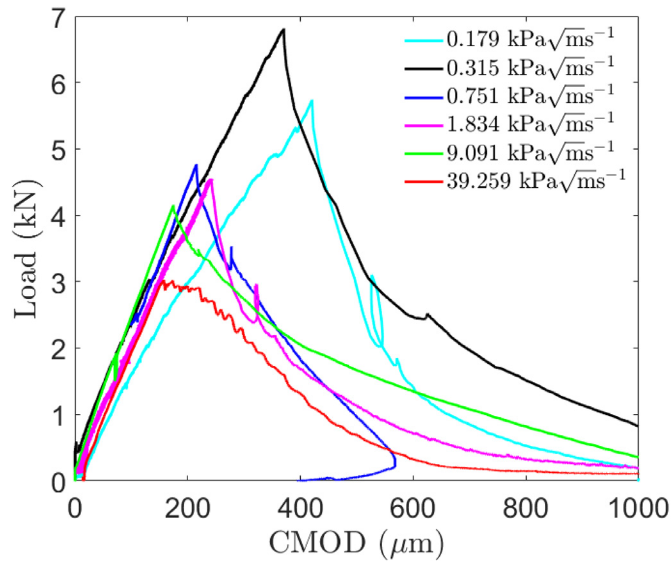

Fig. 4. Load-CMOD records for the 3m x 6m samples with different loading rates. The 39.3 kPa$\sqrt{\text{ms}}^{-1}$ and 1.83 kPa$\sqrt{\text{ms}}^{-1}$ data were smoothed by using moving averages.

Fig. 4 shows the load-CMOD records for the 3m x 6m specimens. A decrease of the peak load with increase in the loading rate is observed. The records show an approximately linear load-displacement relation up to the peak load at high loading rates, but at low loading rates, a non-linear relation is observed.

Fig. 5 shows the apparent fracture toughness (K_Q) and near-crack-tip opening displacements (NCOD1) at the crack growth initiation as functions of loading rate. Interestingly, the data suggests a loading rate dependent size effect for the warm columnar freshwater S2 ice studied: there is a size effect at low rates, but there is no size effect at high rates. At low rates, K_Q and NCOD1 are higher for the large specimen (both 3m x 6m and 19.5m x 36m) than for the small specimen (0.5m x 1m), but with increasing loading rate, the specimen size does not have an effect on K_Q, and NCOD1 for the large specimen approaches the NCOD1 of the small specimen. For both the large and small specimen, K_Q and NCOD1 are decreasing with increasing loading rate, but this rate effect is stronger for the large specimen. This observed size effect is clear between specimens of size 0.5m x 1m and of size 3m x 6m, but there was no size effect between the 3m x 6m specimens and the largest specimen of size 19.5m x 36m. The $K_Q-\dot{K}$ and NCOD1$-\dot{K}$ relations are non-linear and can be well described with a power-law relation.

5.2. Viscoelastic fictitious crack model analysis

The viscoelastic fictitious crack model (VFCM) and the optimization procedure outlined in Section 4 were used to analyze the experimental data. The results are given in Table 2: the number of iterations needed to reach convergence, the five control points defining the $\sigma-\delta$relation (σ_t, σ_1, σ_2, σ_3, δ_c; Fig. 3b), the

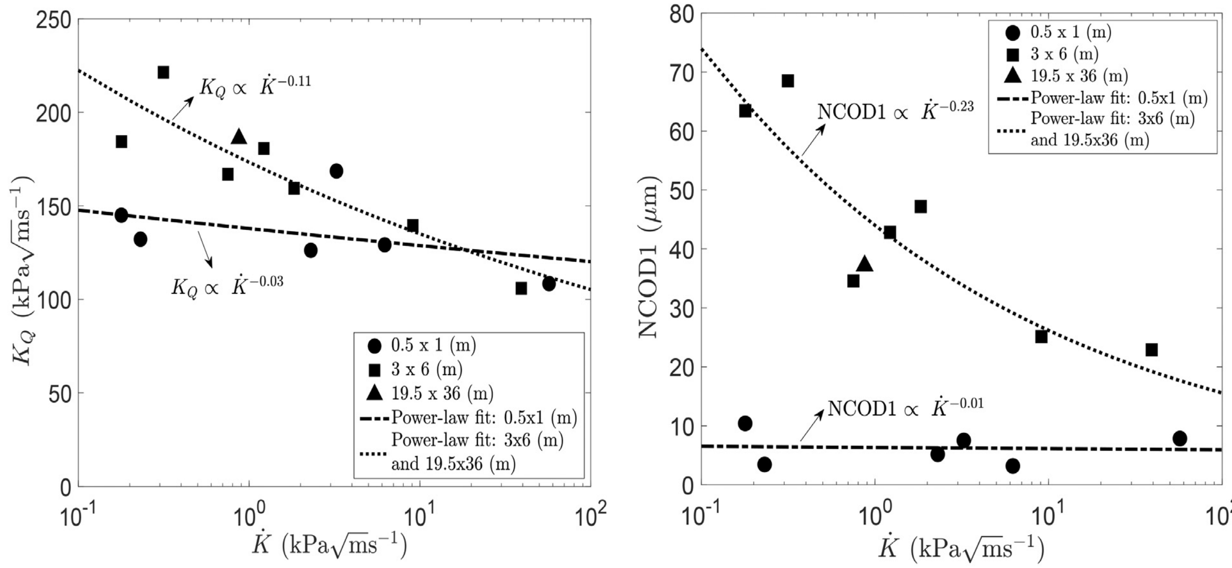

(a) (b)

Fig. 5. Measured apparent fracture toughness (a) and near-crack-tip opening displacements (b) as a function of loading rate. First-order power-law fits were applied to the data. The power-law fits were calculated separately for the larger specimen (both 3m x 6m and 19.5m x 36m) and for the smaller specimen (0.5m x 1m).

Table 2
Optimization results computed using the viscoelastic fictitious crack model.

Test	size (m)	$\dot{K}$ (kPa$\sqrt{\text{ms}}^{-1}$)	Number of iterations	σ_t (MPa)	σ_1 (MPa)	σ_2 (MPa)	σ_3 (MPa)	δ_c (μm)	δ_0 (μm)	Cx 10^{11} ($\text{m}^2\text{N}^{-1}\sqrt{s}^{-1}$)	G_f (N/m)	G_{ac} (N/m)	PZ (mm)	σ_n/σ_t
RP2	0.5x1	3.247	243	1.29	1.29	1.24	1.06	7.09	4.07	5.8	6.54	4.97	6.9	0.509
RP3	0.5x1	57.058	148	1.30	1.30	1.23	0.30	7.57	1.30	3.4	5.48	1.69	2.3	0.332
RP4	0.5x1	6.223	247	1.26	1.26	1.26	1.26	4.44	2.66	6.7	3.42	3.35	4.6	0.401
RP5	0.5x1	0.231	167	1.30	1.28	1.27	1.11	5.27	0.77	4.1	3.63	1.00	1.4	0.402
RP6	0.5x1	0.179	203	1.28	1.28	1.22	0.80	6.73	2.85	3.3	6.49	3.65	5.1	0.456
RP7	3x6	1.834	161	1.30	1.30	1.17	0.54	33.86	3.25	5.2	16.89	4.24	5.9	0.199
RP8	3x6	39.259	688	1.24	1.00	1.00	1.00	18.00	1.44	5.9	14.60	1.78	2.7	0.136
RP9	3x6	1.221	229	1.32	1.22	1.09	0.92	32.80	4.23	5.6	22.30	5.54	6.4	0.222
RP12	3x6	0.315	211	1.02	1.02	1.02	1.02	37.00	8.14	6.2	27.54	8.17	18.4	0.348
RP13	3x6	0.179	130	1.00	1.00	1.00	1.00	40.10	5.69	8.8	30.00	5.69	13.2	0.295
RP14	19.5x36	0.871	476	1.05	1.05	1.05	0.80	36.30	5.58	9.0	20.30	5.83	12.3	0.121

crack opening displacement at crack growth initiation at $X = A_0$ (δ_0), the creep compliance constant (C), the full fracture energy under FDPZ conditions (G_f; Fig. 3b), the actual fracture energy (G_{ac}), and the process zone length (PZ; Fig. 3a). The VFCM analysis required successful measurements of CMOD, COD, and NCOD1 (Fig. 1a) at 15 time instances during the loading. These displacements were small and challenging to measure at the initial, low load levels. Only those experiments, where the whole displacement history was measured successfully, are included in Table 2. Note that Table 1 includes data from all the 14 tests, as the analysis in Table 1 is based on measured maximum values, not on the whole displacement-time record.

Fig. 6 illustrates the correspondence between the experiments and the VFCM for RP14 (19.5m x 36m): the load as measured and as applied to the model, and the response of the ice samples as measured and as obtained from the model. The experiment shows a good agreement between the model results and experimental data. This agreement supports the ability of the VFCM to describe the response of columnar freshwater S2 ice: the VFCM is able to model the non-linear displacement record not only at the crack mouth where the loading is applied (CMOD), but also along the crack (COD) and near the crack tip (NCOD1). The model does not account for crack propagation and thus the comparison is shown up to the peak load only.

Fig. 7 shows the crack opening displacement at crack growth initiation at $X = A_0$ (δ_0), the actual fracture energy (G_{ac}), and the process zone size (PZ) as functions of loading rate. Similar rate and size effects were observed than with the linear elastic fracture mechanics analysis above. The results from the large and mid-size specimens (3m x 6m and 19.5m x 36m) are again interchangeable and higher than the results from the small specimens (0.5m x 1m). This size effect is loading rate dependent and decreases with increasing rate: δ_0, G_{ac}, and PZ for the larger specimen decrease with increasing loading rate and approach the values obtained for the small specimen. No significant rate effect was observed for the small specimen. Power-law relations can be used to describe the decrease of δ_0,G_{ac}, and PZ with rate. Note especially the similarity of size and rate effects between PZ and the measured crack opening displacement near the crack tip in Fig. 5b.

Stress-separation curves were constructed by using the five control points shown in Fig. 3b, and straight lines connecting the points. Fig. 8 shows the back-calculated $\sigma - \delta$ curves under FDPZ conditions and illustrates the impact of the specimen size and loading rate. With increasing separation, the $\sigma - \delta$ curves show initially an approximately constant stress and then extend with a softening behavior, which is getting gradually steeper. This kind of stress-separation curve is similar to what has been observed for sea ice [1]. The data obtained with the larger test size (Fig. 8b) illustrate that with increasing loading rate, the length of the con-

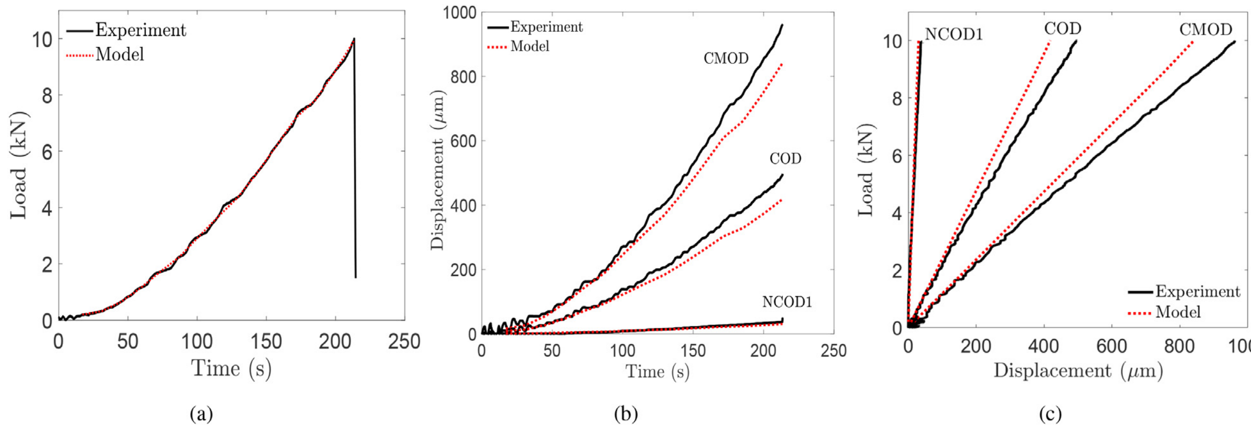

Fig. 6. Experimental and model results for RP14 (19.5m x 36m). (a) Load at the crack mouth, see Fig. 1a and Eq. (1). (b) Displacement - time records. (c) Load - displacement record.

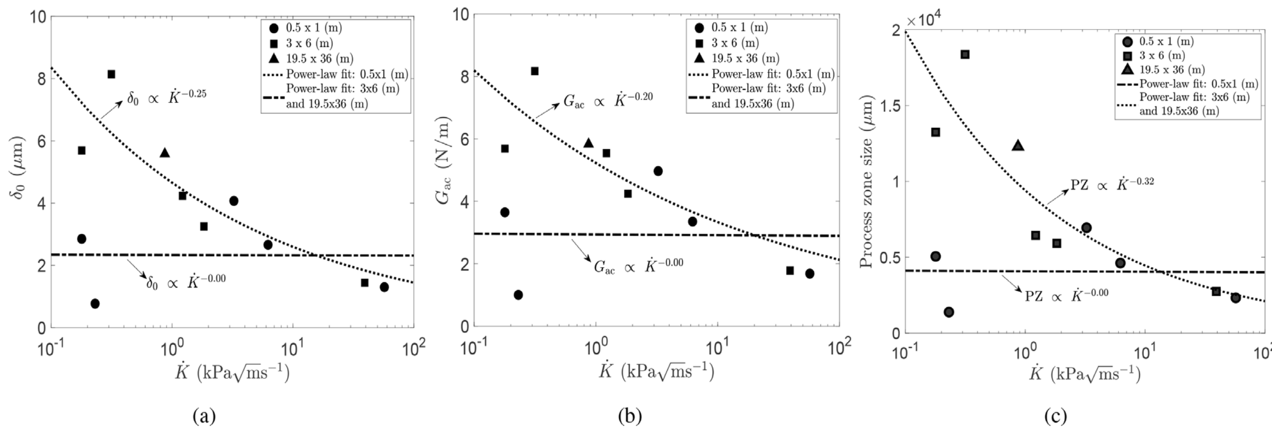

Fig. 7. The crack opening displacement at crack growth initiation at $X = A_0$ (a), the actual fracture energy (b), and the process zone size (PZ) (c) as a function of loading rate. Viscoelastic fictitious crack model was used in the analysis. First-order power-law fits were applied separately to the data for the larger specimen (3m x 6m and 19.5m x 36m) and for the smaller specimen (0.5m x 1m).

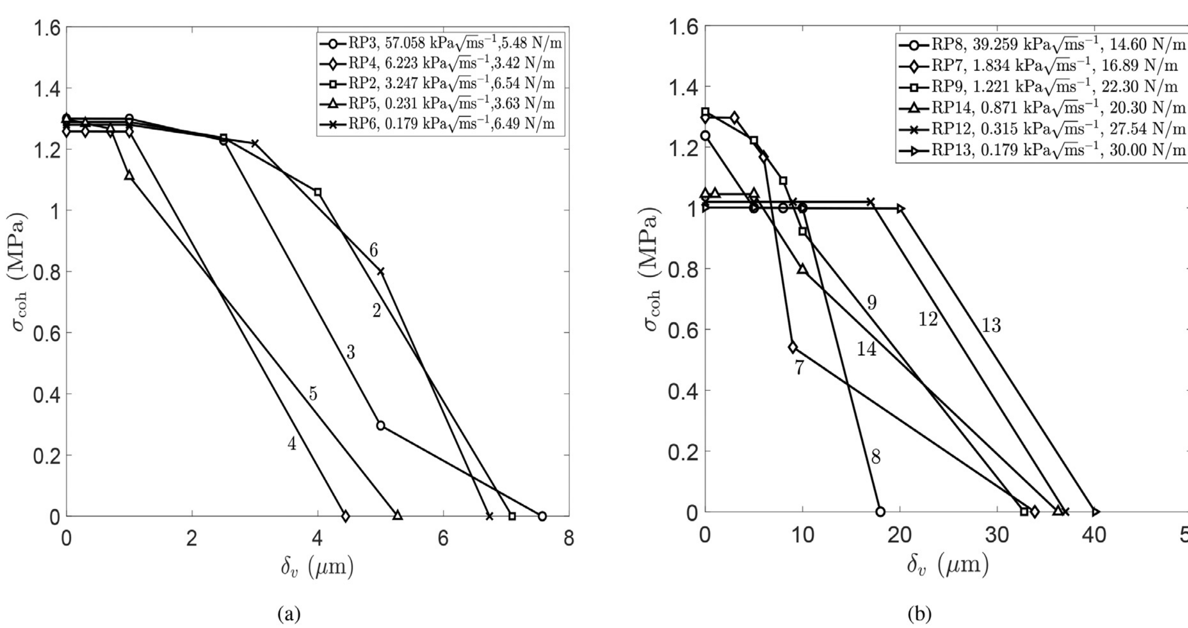

Fig. 8. The stress-separation curves for the 0.5m x 1m specimens (a) and for the 3m x 6m and 19.5m x 36m specimens (b) at different loading rates for the case of fully-developed-process-zones. The number next to each curve reflects the index of the experiment in the Legend.

stant part is decreasing while the slope of the softening part appears less sensitive to the loading rate. This suggests that the observed decrease in fracture energy with loading rate (Fig. 7b) is due to a decrease in the constant part, not due to change in the softening part. At the highest rate studied, no constant part of the stress-separation can be observed, the curve shows more-or-less linear softening only. The stress-separation curves obtained with the small specimens (Fig. 8a) show similar behaviour, but not as clearly. Although the experiments were conducted under displacement control, none of them realized a FDPZ, and the experiments fractured at peak load. Only a portion of the stress-separation curve (Fig. 8) and the fracture energy (G_f,Table 2) was attained prior to the initiation of crack growth. It is possible that the very high homologous test temperatures and the inevitable grain boundary melting [40] are the reason for not attaining a FDPZ. The change in the shape of the $\sigma - \delta$ curve with loading rate is an indication of changes in the deformation and fracture processes with rate. At low rates, the approximately constant initial part of the $\sigma - \delta$ curve indicates that the freshwater ice deforms initially without softening and the material inside the cohesive zone is able to transfer the full tensile strength for some time with increasing load, until the deformation becomes so large that softening starts and finally leads to extension of the physical, traction-free crack. At high rates, no constant part of the curve is observed and softening initiates immediately when the critical stress is reached. This explains why freshwater ice appears brittle at high loading rates and less brittle at low rates.

The stress-separation curve includes the tensile strength (σ_t) of the ice studied (Fig. 8). This value was not as strongly or clearly affected by specimen size or loading rate as the fracture parameters: for the small specimen $\sigma_t \approx 1.3$ MPa, for the large specimen $\sigma_t = 1.0 \cdots 1.3$ MPa, higher for the higher rates.

5.3. Notch sensitivity analysis

The dependence of notch sensitivity on specimen size was discussed by Carpinteri [41] for concrete fracture. Notch sensitivity is given by the ratio between the peak nominal tensile stress (σ_n) at the crack tip and the tensile strength (σ_t) of an uncracked specimen. This ratio is function of the brittleness number β_t which is used to test that a fracture test is notch sensitive and the validity of LEFM [3]. Formulations of the notch sensitivity for the edge-cracked rectangular geometry with the current loading configuration are outlined in Appendix A. Table 2 gives the notch sensitivity values for the different tests, computed using the σ_n and σ_t values listed in Table 1 and Table 2, respectively.

Figs. 9a, 9b, and 9c show the σ_n/σ_t versus the normalized crack length for the 0.5m x 1m, 3m x 6m, and 19.5m x 36 m specimens, respectively. Lines of constant brittleness numbers are shown. The crack length of each specimen size is indicated by the vertical dashed line. It is evident that the fracture tests completely lose their meaning if $\sigma_n = \sigma_t$: a strength failure occurs prior to the attainment of a critical SIF. For the 0.5m x 1m and 3m x 6m specimens, that occurs for β_t higher than $\beta_t^0 \approx 0.36$; for the largest specimen $\beta_t^0 \approx 0.33$ (Fig. 9). This is shown by the intersection of the horizontal dashed line of $\sigma_n/\sigma_t = 1$and the vertical dashed line. For values of $\beta_t < \beta_t^0$,the fracture tests are more significant for shorter cracks. However, the selection of the optimum crack length should ensure simultaneously a polycrystalline behavior and a high enough degree of brittleness (low enough σ_n/σ_t) for a given specimen size.

More importantly, the brittleness number can reveal the optimum specimen size so that the tests are significant ($\beta_t < \beta_t^0$) and suitably notch sensitive ($\sigma_n/\sigma_t << 1$) which further restricts β_t. Considering size effect, previous analyses showed that the results of the two larger, 3m x 6m and 19.5m x 36m, samples were interchangeable, suggesting from Figs. 9b and 9c that a $\sigma_n/\sigma_t <$ 0.4 is good enough to generate size-independent fracture results. Dempsey [3] proposed the same ratio to ensure notch sensitivity and referred to it as the specimen shape-independent condition. It is worth noting that the 0.5m x 1m, 3m x 6m, and 19.5m x 36m plates are 77x, 462x, and 3000x the grain size, respectively. Mulmule and Dempsey [42] speculated that sample homogeneity for first-year sea ice would be obtained if the crack-parallel specimen size harboured at least 200 d_{av},where $d_{av}$is the average grain size. These tests for very warm S2 columnar ice suggest that a crack-parallel specimen size of about 460 d_{av}would be required for polycrystalline homogeneity. This highlights the huge difference posed by the testing of cracked and uncracked test samples. For the tensile and compressive testing of un-notched ice cylinders, it is recommended that the cylinder diameter be 15 to 20 times d_{av}[43]. However, as soon as one is testing a cracked test sample, the requisite specimen size is measured not in 10's of the grain size, but 100's of the grain size.

Considering the rate effect further restricts the notch sensitivity requirement. Fig. 9d extends this analysis by showing the variation of σ_n/σ_t as a function of loading rate. First-order power-law fits were applied to the data for the 0.5m x 1m and 3m x 6m specimens. The 3m x 6m specimens displayed a higher rate effect than the 0.5m x 1m specimens which satisfied the shape-independent condition only at high rates. For the 3m x 6m specimens: at low rate, the suggested $\sigma_n/\sigma_t < 0.4$ is valid; while at higher rates, a much lower ratio of $\sigma_n/\sigma_t < 0.2$ is necessary to ensure notch sensitivity. The discussion of notch sensitivity in terms of both size and rate further limits the brittleness condition to $\sigma_n/\sigma_t < 0.2$. The effect of rate on notch sensitivity has not been discussed before. A tentative conclusion is that the selection of the optimal specimen size and crack length, for LEFM applicability, should consider simultaneously polycrystalline homogeneity and notch sensitivity, including the effects of size and rate.

6. Discussion

The observed fracture characteristics of S2 columnar freshwater ice are reminiscent of what is expected of quasi-brittle materials, such as concrete and rock [44]. An important consequence is that the thickness of the specimen (i.e. the length of the crack front) is not an important variable for the fracture of freshwater ice, as has been shown for the fracture of concrete [44,45]. The direct consequence is that there is no validity to plane stress and plane strain idealizations, which proved very important to the development of the metals-based fracture mechanics [46]. For long crack fronts, a triaxial state of stress does not materialize, as the tensile stress parallel to the crack front is relieved by microcracking parallel to the top and bottom surfaces or by creep, the latter taking place rapidly.

The fracture experiments conducted with columnar freshwater S2 ice showed both size and rate effects which can be expressed either as a rate dependent size effect or as a size dependent rate effect. There was a size effect at the lower rates but no size effect at the higher rates. There was a rate effect for the larger specimens but a weak or no rate effect for the smaller specimens. This interrelation of size and rate effects for columnar freshwater ice is a novel observation; earlier experiments have observed rate effects [7,9–11,15–17,22,23] or size effects [1,2,6,25], but not how these two are related. In addition, the rate dependency of fracture energy has not been reported earlier: fracture energy increases with decreasing loading rate (Fig. 7b). Compared with the earlier studies with freshwater S2 ice, the specimens tested here were large ($L \geq 0.5$)m, very warm (≥ -0.35 C), and tested *in-situ*.

The apparent fracture toughness (K_Q) measured – about 100 kPa$\sqrt{\mathrm{m}}$ at high rates and about $100 - 200$ kPa$\sqrt{\mathrm{m}}$ at low rates –

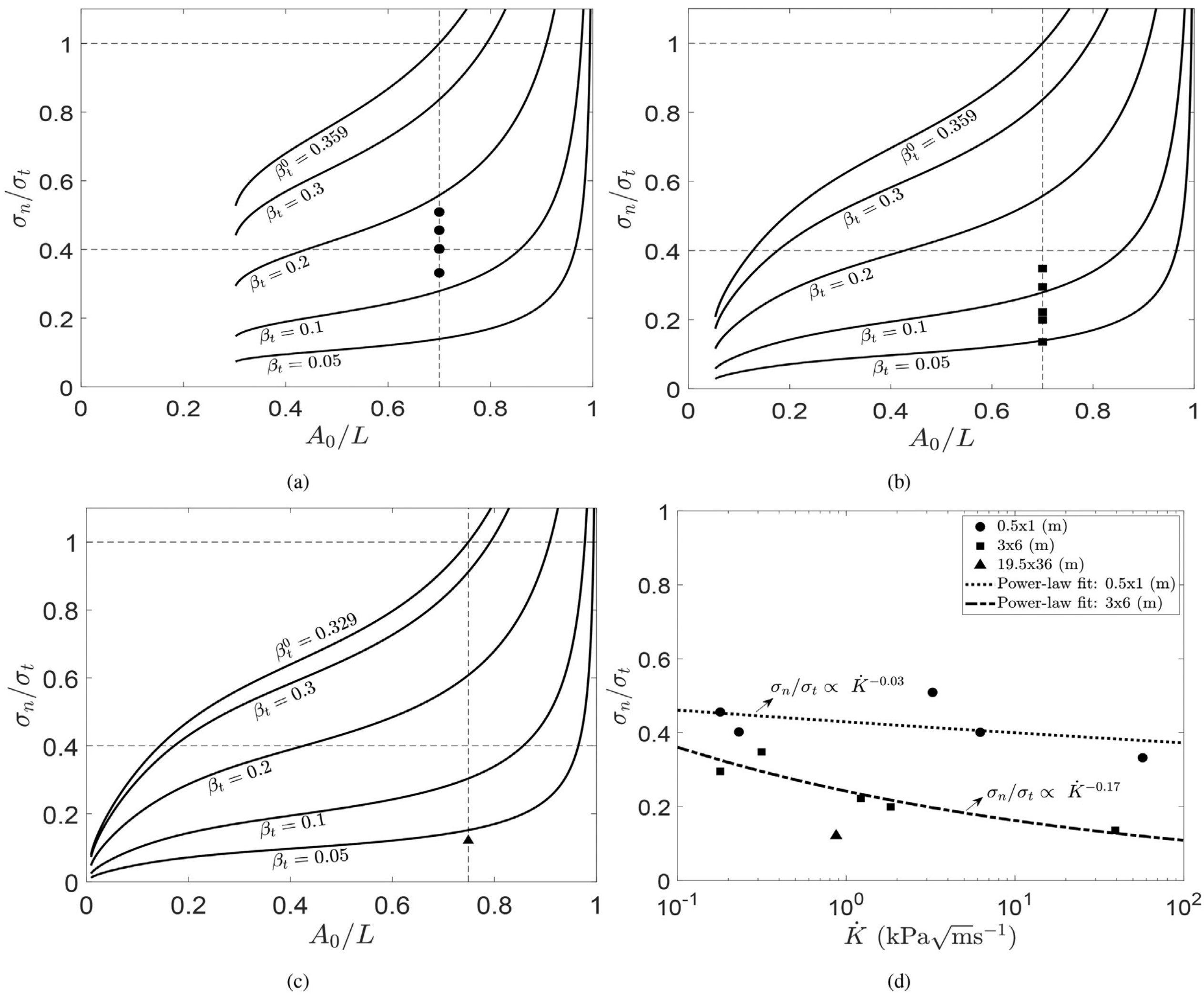

Fig. 9. Notch sensitivity (σ_n/σ_t) as a function of the normalized crack length for the 0.5m x 1m (a), 3m x 6m (b), and 19.5m x 36 m (c) specimens. Lines of constant brittleness numbers are shown. The notch sensitivity of $\sigma_n/\sigma_t = 0.4, 1$ are indicated with the horizontal dashed lines. The normalized crack length of each specimen size is shown by the vertical dashed line. (d) Notch sensitivity (σ_n/σ_t) as a function of the loading rate. First-order power-law fits were applied to the data for the 0.5m x 1m and 3m x 6m specimens.

is within the range measured earlier for columnar S2 freshwater ice [3]. While values for K_Q are given in Table 1 and Fig. 5a, the validity of K_Q as a material parameter for ice should be discussed. K_Q is an LEFM parameter and thus limited to be used when the material response can be idealised as linearly elastic, except in a small *process zone* near the crack tip, where *yielding* – or in the case of ice, *microcracking* and *creep* – may occur [47]. If such a process zone is small enough compared with the other dimensions of the specimen, fracture toughness governs crack growth; if a specimen experiences extensive yielding or creep – near the crack tip or elsewhere in the specimen – fracture toughness is not a relevant parameter.

The size of the process zone in ice has been estimated with different methods. Following Riedel and Rice [47], who studied tensile cracks in elastic-nonlinear viscous materials, a creep zone size for freshwater ice has been estimated to be in the range of $0.01 \cdots 0.5$ mm at a rate of about 2 kPa$\sqrt{\text{m}}$s^{-1} and temperatures of -10 C or lower [15,16,24]. It is important to note that the elastic power-law model of Riedel and Rice is applicable to materials where considerable ductility is present in the process zone. Another method used for ice is the method suggested by Veerman and Muller [48], where the size of a plastic zone near a crack tip is related with the location of an apparent rotation axis of a specimen in bending. For specimen with the largest dimension of 0.4 m, a rate of 2 kPa$\sqrt{\text{m}}$s^{-1} and temperature of -5 C, this method has suggested a process zone size of about 0.5 mm [22,23]. These results of a small process zone have led to conclusions that LEFM is a suitable model for ice fracture at the rates and temperatures studied. However, the above values are an order of magnitude smaller than the about 5 mm measured here at the same rate but with larger specimens and warmer ice (Fig. 7c). The PZ measured here for freshwater ice, about 5 – 15 mm depending on rate and specimen size, is again an order of magnitude smaller than the PZ measured for sea ice: about 25 mm for 1 m specimen and up to 150 mm for test sizes larger than 3 m [1]. The size of the freshwater fracture process zone, as with many ice parameters, is affected by scale, rate, and temperature. Rodin and coworkers [49,50] studied similar polycrystalline S2 warm ice and modelled the plate as a single grain specimen governed by the crack tip's location and loaded through a metal-ice composite testing machine. Their model anticipated smaller PZ size than the grain size. However, the current observed PZ sizes are significant and are of the order of the grain size if not multiple times the grain size, especially as the specimen gets larger with the 3m x 6m and 19.5m x 36 m specimens. This concludes that the one grain ice-metal system envisaged by Rodin and coworkers is not applicable in this case.

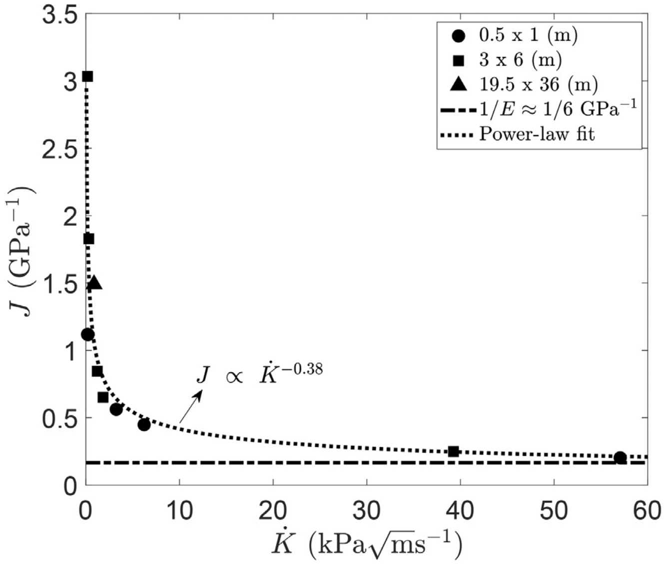

Fig. 10. Variation of creep compliance ($J = 1/E + Ct^{1/2}$) as a function of loading rate ($\dot{K}$) for different specimen sizes.

Freshwater ice is a viscoelastic material, and it can be hypothesised that the viscous deformation is less significant when the loading rate is high, and the temperature is low. Quantitively the elastic and viscous responses can be analysed by using the non-linear viscoelastic model (VFCM) and especially the creep compliance ($J = 1/E + Ct^{\frac{1}{2}}$). J, calculated for each experiment by using $E = E_{\text{CMOD}}$, $t = t_f$, and $C$from Tables 1 and 2, is shown in Fig. 10 as a function of the loading rate. Note that both $E$and C show some scatter but not a relation with the loading rate. As J is a function of time, a rate effect is observed, but interestingly, J appears not to have size effect – at least the size effect is much weaker than for the other parameters studied here. At high loading rates, J approaches the value of $1/E$ (elastic compliance), but with decreasing loading rate, the viscous component of J increases and the material response deviates more and more from an elastic behavior. At loading rates $\dot{K} \approx 20\text{kPa}\sqrt{\text{m}}\,\text{s}^{-1}$ or less, J is twice or more of the elastic compliance. Thus, the warm freshwater ice studied here can be considered elastic only when $\dot{K}$is higher than about 50 kPa$\sqrt{\text{m}}\,\text{s}^{-1}$; or the time to failure is less than $1-2$ seconds. This strongly supports the notch sensitivity ratio ($\sigma_n/\sigma_t < 0.2$), suggested in Section 5.3, for LEFM applicability. For other types of ice and for other temperatures, different limit rates for elastic response should be found. Earlier studies, based on analysis of the process zone size, have concluded that LEFM is a valid fracture model when $\dot{K} > 10$ kPa$\sqrt{\text{m}}\,\text{s}^{-1}$[11,16], suggesting a larger range for LEFM than suggested here.

Finally, it is interesting to note that the tensile strength (σ_t), obtained from the experimental data through the VFCM analysis, was about 1.2 MPa (Fig. 8) and not as strongly affected by size or rate as the fracture parameters. In earlier experiments tensile strength of ice has been observed to be a function of temperature, grain size, orientation, porosity – all constants in the experiments reported here – but also of strain rate [51]. Why the tensile strength, as defined in the VFCM, does not show a clear rate effect when it has been measured before, and when the other fracture parameters do show both rate and size effects?

7. Summary and conclusions

Laboratory experiments on size (scale) and rate effects on the fracture behavior of warm, columnar (S2), freshwater ice were completed at the Aalto Ice Tank. The samples covering a size range of 1 : 39 were edge-cracked rectangular floating plates loaded at the crack mouth; the largest sample had dimensions of 19.5m x 36m. This size and the size range are to our knowledge the largest for ice under laboratory conditions. The loading rates applied led to loading durations from fewer than 2 seconds to more than 1000 seconds leading to an elastic response at the highest rates and a viscoelastic response at the lower rates. The tests were displacement controlled and monotonically loaded up to fracture. The fracture mode was transgranular in all the experiments.

The experiments were analysed by using the linear-elastic fracture mechanics (LEFM) and the non-linear viscoelastic fictitious crack model (VFCM) approach. For the LEFM analysis, expressions for the apparent fracture toughness (K_Q) and crack opening displacement were derived by following the weight function method by Dempsey and Mu [30]. For the VFCM, the approach formulated by Mulmule and Dempsey [32] was adopted and combined with the Nelder-Mead optimization scheme [36] to back-calculate the constitutive parameters: stress-separation curve, fracture energy, creep compliance constant, and size of the fracture process zone (PZ).

The main observation from the experiments is that the size and rate effects were interrelated. There was a size effect at low loading rates, but no size effect was observed at the higher rates. This applied to the crack opening displacement near the crack tip (NCOD1) as measured, to K_Q as an LEFM parameter, as well as to the stress-separation curve, G_{ac} and PZ as VFCM parameters. The rate dependent size effect is a novel result for any type of ice. Earlier both rate effects and size effects have been measured, but not how these two are related. Similar to earlier studies, the rate effects – when observed – followed power law type relations. The rate dependent size effect can be related with the fracture process at the vicinity of the crack tip: Both the measured NCOD1 and the calculated PZ of the larger specimen decrease with increasing rate and approach the values for the smaller specimen. As was illustrated by using the VFCM, the ice studied can be considered elastic only at the highest rates applied, the rates where the size effect vanishes.

The measured size and rate effects can be expressed also as size dependent rate effects. For the larger specimen (3m x 6m and 19.5m x 36m), a clear rate effect was observed, while for the small specimen (0.5m x 1m) the rate effect was weak or absent.

The results of the two larger, 3m x 6m and 19.5m x 36m, samples were interchangeable suggesting that the 3m x 6m sample size is large enough to give size-independent fracture results for this type of warm ice. From the experimental results and analysis presented, the following requirements are recommended.

$$L/d_{\text{av}} \geq 460 \quad \text{polycrystalline homogeneity requirement},$$

$$\sigma_n/\sigma_t < 0.2 \quad \text{notch sensitivity},$$

in which L is the specimen size in the cracking direction, as portrayed in Fig. 1a and d_{av} is a measure of the average grain size. The crack length must be selected to optimize the brittleness of the test plate.

This study proved that the viscoelastic fictitious crack model is successful in treating the fracture of S2 columnar freshwater ice.

Declaration of Competing Interest

None.

Acknowledgements

This work was funded though the Finland Distinguished Professor programme “Scaling of Ice Strength: Measurements and Modeling", and through the ARAJÄÄ research project, both funded by Business Finland and the industrial partners Aker Arctic Technology, Arctech Helsinki Shipyard, Arctia Shipping, ABB Marine, Finnish Transport Agency, Suomen Hyötytuuli Oy, and Ponvia Oy. This financial support is gratefully acknowledged. The authors express their appreciation to Dr. Mikko Suominen and Teemu Päivärinta for their efforts in growing columnar freshwater S2 ice at the Aalto Ice Tank. The authors acknowledge the original idea of Dr. Otto Puolakka who introduced the use of a milling machine for thinning the ice. The first author (I.E.G.) would like to thank Dr. Mohamad Gharamti for his useful advice and help on various numerical issues examined in this paper. The second author (J.P.D.) thanks Business Finland for support by the FiDiPro Professorship from Aalto University, and the sabbatical support from Aalto University, which collectively supported an annual visit 2015-2016, and summer visits 2017-2019.

Appendix A. Mathematical Details

For the edge-cracked rectangular geometry with the current loading configuration, the nominal stress is given by

$$\sigma_n = \frac{2P_{\max}}{hL} g(a_0), \quad g(a_0) = \frac{2 + a_0 - 3d/2}{(1 - a_0)^2} \tag{A1}$$

Using $P_{\max}$ provided in Eq. (1), it follows that

$$\frac{\sigma_n}{\sigma_t} = C_n \beta_t \tag{A2}$$

in which

$$\beta_t = \frac{K_{Ic}}{\sigma_t \sqrt{L}}, \quad C_n = \frac{d\sqrt{2\pi}}{\sqrt{a_0} Z_1(d, a_0)} g(a_0) \tag{A3}$$

Note that β_t as used in the paper is expressed in terms of Dempsey's notation of K_Q (Eq. (1)) instead of K_{Ic}, given that no standard exists for K_{Ic}.

Finally, in Section 3,

$$Z_1(d, a_0) = \sum_{i=1}^{5} \frac{\mathcal{G}_i(a_0)}{2i - 1} \left(1 - \left(1 - \frac{d}{a_0}\right)^{i - \frac{1}{2}}\right) \tag{A4}$$

$$Z_2(x, \eta) = \sum_{i=1}^{5} \mathcal{G}_i(\eta) \left(1 - \frac{x}{\eta}\right)^{i - \frac{3}{2}} \tag{A5}$$

where $\mathcal{G}_i$(i = 1,2,...,5) are functions given by Eq. (4) in [30].

References

[1] S.V. Mulmule, J.P. Dempsey, Scale effects on sea ice fracture, Mechanics of Cohesive-frictional Materials 4 (1999) 505–524.
[2] J.P. Dempsey, D.M. Cole, S. Wang, Tensile fracture of a single crack in first-year sea ice, Philosophical Transactions of the Royal Society A 376 (2129) (2018) 20170346.
[3] J.P. Dempsey, The fracture toughness of ice, in: Ice-structure interaction, Springer, Berlin, Heidelberg, 1991, pp. 109–145.
[4] K. Abdel-Tawab, G.J. Rodin, On the relevance of linear elastic fracture mechanics to ice, International Journal of Fracture 62 (2) (1993) 171–181.
[5] K. Abdel-Tawab, G.J. Rodin, Fracture size effects and polycrystalline inhomogeneity, International Journal of Fracture 93 (1-4) (1998) 247–259.
[6] J.P. Dempsey, S.J. DeFranco, R.M. Adamson, S.V. Mulmule, Scale effects on the in-situ tensile strength and fracture of ice. Part I: Large grained freshwater ice at Spray Lakes Reservoir, Alberta, International Journal of Fracture 95 (1999) 325–345.
[7] H.W. Liu, W. Loop, Fracture toughness of freshwater ice. CRREL Technical Note, USA Cold Regions Research and Engineering Laboratory, 1972.
[8] D.J. Goodman, D. Tabor, Fracture toughness of ice: a preliminary account of some new experiments, Journal of Glaciology 21 (1978) 651–660.
[9] H.W. Liu, K.J. Miller, Fracture toughness of fresh-water ice, Journal of Glaciology 22 (1979) 135–143.
[10] H. Hamza, D.B. Muggeridge, Plane strain fracture toughness (K_{1c})of fresh water ice, in: International Conference on Port and Ocean Engineering under Arctic Conditions, volume 1, 1979, pp. 697–707.
[11] N. Urabe, A. Yoshitake, Strain rate dependent fracture toughness (K_{1c})of pure ice and sea ice, in: Proceedings of the 6th IAHR Symposium on Ice, Quebec City, PQ, Canada, volume 2, 1981, pp. 551–563.
[12] G.W. Timco, R. Frederking, Comparative strengths of fresh water ice, Cold Regions Science and Technology 6 (1982) 21–27.
[13] V.I. Danilenko, Determination of crack resistance (K_{1c})of freshwater ice, Mechanics of Solids 20 (1985) 131–136.
[14] B.L. Parsons, J.B. Snellen, Fracture toughness of fresh water prototype ice and carbamide model ice, in: 8th International Conference on Port and Ocean Engineering under Arctic Conditions, Narsarsuaq, Greenland, volume 1, 1985, pp. 128–137.
[15] G.W. Timco, R.M.W. Frederking, The effects of anisotropy and microcracks on the fracture toughness (K_{1c})of freshwater ice, in: Proceedings of the 5th International OMAE Symposium, Tokyo, Japan, volume 4, 1986, pp. 341–348.
[16] W.A. Nixon, E.M. Schulson, Fracture toughness of freshwater ice as a function of loading rate, in: Proceedings of the 1st International Conference on Ice Technology, Cambridge, MA, 1986, pp. 287–296.
[17] J. Tuhkuri, The applicability of LEFM and the fracture toughness (K_{Ic})to sea ice, in: The 9th International Conference on Port and Ocean Engineering under Arctic Conditions, Fairbanks, Alaska, volume 1, 1987, pp. 21–32.
[18] D.L. Bentley, J.P. Dempsey, D.S. Sodhi, Y. Wei, Fracture of S2 columnar freshwater ice: floating double cantilever beam tests, in: Proceedings of the 9th International IAHR Symposium on Ice, Sapporo, Japan, volume 1, 1988, pp. 152–161.
[19] J.P. Dempsey, Y. Wei, S. DeFranco, R. Ruben, R. Frachetti, Fracture toughness of S2 columnar freshwater ice: crack length and specimen size effects – part II, in: The 10th International Conference on Port and Ocean Engineering under Arctic Conditions, Luleå, Sweden, volume 1, 1989, pp. 199–207.
[20] B.L. Parsons, J.B. Snellen, D.B. Muggeridge, The double torsion test applied to fine grained freshwater columnar ice and sea ice, Mechanics of Creep Brittle Materials 1 (1989) 188–200.
[21] Y. Wei, S.J. DeFranco, J.P. Dempsey, Crack-fabrication techniques and their effects on the fracture toughness and CTOD for fresh-water columnar ice, Journal of Glaciology 37 (1991) 270–280.
[22] L.J. Weber, W.A. Nixon, Fracture toughness of freshwater ice – Part I: Experimental technique and results, Journal of Offshore Mechanics and Arctic Engineering 118 (1996) 135–140.
[23] L.J. Weber, W.A. Nixon, Fracture toughness of freshwater ice – Part II: Analysis and micrography, Journal of Offshore Mechanics and Arctic Engineering 118 (1996) 141–147.
[24] X. Xu, G. Jeronimidis, A.G. Atkins, P.A. Trusty, Rate-dependent fracture toughness of pure polycrystalline ice, Journal of Materials Science 39 (2004) 225–233.
[25] J.P. Dempsey, R.M. Adamson, S.V. Mulmule, Scale effects on the in-situ tensile strength and fracture of ice. Part II: First-year sea ice at Resolute, N.W.T, International Journal of Fracture 95 (1999) 347–366.
[26] B. Michel, R.O. Ramseier, Classification of river and lake ice, Canadian Geotechnical Journal 8 (1971) 36–45.
[27] D.M. Cole, Effect of grain size on the internal fracturing of polycrystalline ice. CRREL Report 86-5, USA Cold Regions Research and Engineering Laboratory, 1986.
[28] W.B. Kamb, Refraction corrections for universal stage measurements. I. uniaxial crystals, American Mineralogist: Journal of Earth and Planetary Materials 47 (1962) 227–245.
[29] C.C. Langway, Ice fabrics and the universal stage. CRREL Technical Report 62, USA Cold Regions Research and Engineering Laboratory, 1958.
[30] J.P. Dempsey, Z. Mu, Weight function for an edge-cracked rectangular plate, Engineering Fracture Mechanics 132 (2014) 93–103.
[31] A. Hillerborg, M. Modéer, P.-E. Petersson, Analysis of crack formation and crack growth in concrete by means of fracture mechanics and finite elements, Cement and Concrete Research 6 (1976) 773–781.
[32] S.V. Mulmule, J.P. Dempsey, A viscoelastic fictitious crack model for the fracture of sea ice, Mechanics of Time-Dependent Materials 1 (1997) 331–356.
[33] M. Elices, G.V. Guinea, J. Gomez, J. Planas, The cohesive zone model: advantages, limitations and challenges, Engineering Fracture Mechanics 69 (2002) 137–163.
[34] D.M. Cole, The effect of creep on the constitutive behavior of saline ice at low strains, in: Ice Mechanics-1993, volume 163, ASME AMD, 1993, pp. 261–272.
[35] R.A. Schapery, Viscoelastic deformation behavior of ice based on micromechanical models, in: Ice Mechanics-1993, volume 163, ASME AMD, 1993, pp. 15–33.
[36] J.A. Nelder, R. Mead, A simplex method for function minimization, The Computer Journal 7 (1965) 308–313.
[37] D. Carter, B. Michel, Ph.D. Thesis: Lois et mecanismes de l'apparente fracture fragile de la glace de riviere et de lac, Universite Laval, Section Mecanique des Glaces, 1971.
[38] L.W. Gold, Engineering properties of fresh-water ice, Journal of Glaciology 19 (1977) 197–212.
[39] B. Michel, The strength of polycrystalline ice, Canadian Journal of Civil Engineering 5 (1978) 285–300.
[40] J.G. Dash, A.W. Rempel, J.S. Wettlaufer, The physics of premelted ice and its geophysical consequences, Reviews of modern physics 78 (3) (2006) 695.
[41] A. Carpinteri, Notch sensitivity in fracture testing of aggregative materials, Engineering Fracture Mechanics 16 (1982) 467–481.
[42] S.V. Mulmule, J.P. Dempsey, LEFM size requirements for the fracture testing of sea ice, International Journal of Fracture 102 (1) (2000) 85–98.
[43] J. Schwarz, R. Frederking, V. Gavrillo, I.G. Petrov, K.-I. Hirayama, M. Mellor, P. Tryde, K.D. Vaudrey, Standardized testing methods for measuring mechanical properties of ice, Cold Regions Science and Technology 4 (3) (1981) 245–253.

[44] A. Hillerborg, Analysis of one single crack, in: Fracture Mechanics of Concrete, Elsevier, Amsterdam, 1983, pp. 223–249.
[45] S. Mindess, J.S. Nadeau, Effect of notch width on (K_{1c}) for mortar and concrete, Cement and Concrete Research 6 (4) (1976) 529–534.
[46] D. Broek, Elementary Engineering Fracture Mechanics, Noordhoff Publishing Co., Leiden, 1974.
[47] H. Riedel, J.R. Rice, Tensile cracks in creeping solids, in: Fracture Mechanics. Proceedings of the Twelfth National Symposium on Fracture Mechanics, ASTM STP 700, 1980, pp. 112–130.
[48] C.C. Veerman, T. Muller, The location of the apparent rotation axis in notched bend testing, Engineering Fracture Mechanics 4 (1972) 25–32.
[49] G.J. Rodin, On fracture of warm ice, in: IUTAM Symposium on Scaling Laws in Ice Mechanics and Ice Dynamics, Springer, 2001, pp. 207–216.
[50] Y. Wang, R. Ballarini, G.J. Rodin, Crack-tip parameters in polycrystalline plates with soft grain boundaries, Journal of Engineering Mechanics 134 (1) (2008) 100–109.
[51] E.M. Schulson, P. Duval, Creep and Fracture of Ice, Cambridge University Press, 2009.